REDVET - Revista electrónica de Veterinaria - ISSN 1695-7504
Vol 24, No.4 (2023) http://www.veterinaria.org
Article Received: September 2023; Revised: October 2023; Published: November 2023

Advancing Diabetic Retinopathy Detection: Integrating Deep Learning and Texture Analysis for Enhanced Lesion Identification

Shubhi Shrivastava[1*], Dr. Shanti Rathore[2], Dr. Rahul Gedam[3], Dr. Sharda Pratap Shrivas[4]

[1*]Research Scholar, Electronics And communication Department, Dr. C V Raman University, Kota Bilaspur, shubhi@lcit.edu.in,
[2]Associate Professor, Electronics And communication Department, Dr. C V Raman University, Kota Bilaspur, rathoreshanti@gmail.com,
[3]Associate Professor, Electronics And Telecommunication Department, LCIT, Bilaspur, : engg.rahul2801@gmail.com
[4]Assistant Professor, Department of Mechanical Engineering, Chouksey Engineering College Bilaspur

Abstract –The proposed work intends to automate the detection and classification of diabetic retinopathy from retinal fundus image which is very important in ophthalmology. Most of the existing methods use handcrafted features and those are fed to the classifier for detection and classification purpose. Recently convolutional neural network (CNN) is used for this classification problem but the architecture of CNN is manually designed. This paper proposes a novel methodology that combines deep learning techniques with texture analysis to enhance the accuracy of retinal lesion detection. The proposed methodology integrates Convolutional Neural Network (CNN)-based deep features extraction with Gray-Level Co-occurrence Matrix (GLCM) texture features extraction. Additionally, a feature fusion process and Neighborhood Component Analysis (NCA)-based feature selection are employed to optimize the feature representation. The classification stage utilizes Support Vector Machine (SVM) to classify retinal images based on the extracted features. Simulation results and discussions on the DRIVE dataset demonstrate the effectiveness of the proposed methodology, achieving an accuracy of 99.07% and demonstrating superior performance compared to previous research works.

Keywords **–** Convolutional Neural Network, Diabetes Mellitus, Diabetic Retinopathy, Gray-Level Co-occurrence Matrix, Neighborhood Component Analysis, Support Vector Machine.

I. INTRODUCTION

Diabetes mellitus (DM) is a prevalent chronic condition, ranking as the fourth leading cause of death globally. According to recent estimates by the International Diabetes Federation (IDF), approximately 336 million people worldwide have DM, with projections indicating a potential increase of up to 7.7% by 2030 [1]. Diabetic retinopathy (DR) is a serious complication of DM, leading to irreversible blindness in adults worldwide. This condition is associated with both type 1 and type 2 diabetes, with a high prevalence among patients who have had diabetes for extended periods. For instance, 75-95% of type 1 diabetes patients with a 15-year history exhibit signs of DR, while 60% of type 2 diabetes patients with over 16 years of illness are affected [2]. Globally, DR affects approximately 80% of patients diagnosed with diabetes for more than ten years [3]. Its rapid progression, often without early symptoms, underscores the importance of early screening, proper medication, and consistent treatment to mitigate its prevalence. Various societies recognize the value of initial treatment procedures for DR diagnosis, including point-of-care ophthalmoscopy through fundus photography and centralized grading in screening applications. Despite growing evidence supporting routine assessment and early intervention, real-time DR screening remains limited, particularly in developing countries. This limitation is primarily due to a shortage of trained retinal experts and inadequate financial resources to address the increasing prevalence of diabetes [4]. Digital fundus imaging serves as a standard diagnostic tool for DR, with recent clinical studies recommending periodic examinations throughout a diabetic patient's lifetime. These examinations vary in frequency based on the severity of DR, with annual screenings suggested for patients with no or mild DR and more frequent assessments for those with moderate retinopathy. Between 2000 and 2010, there was a notable shift in the incidence of blindness due to diabetes in England and Wales [5]. This increase in demand for care has prompted a transition from traditional physician-led treatment approaches to computer-aided diagnosis (CAD) systems. These CAD programs are expected to achieve competitive sensitivity (SE) and specificity (SP) rates compared to expert evaluations. In the UK, diabetes recommendations stipulate that CAD systems should have a minimum SE of 80%. The adoption of automated analysis systems has significantly reduced workload, with a 61.2% decrease in distinguishing healthy samples from those with diabetic retinopathy [5]. These computerized systems demonstrate diagnostic capabilities comparable to expert evaluators, while potentially offering superior abilities in detecting disease progression and classifying stages. Furthermore, their robust image analysis output remains consistent over time, even in the presence of transient criterion changes and low-quality images.

Deep learning models (DLMs), a subset of machine learning, have emerged as powerful tools in various domains, including computer vision and biomedical imaging analysis. Deep convolutional neural networks (CNNs), a popular type of DLM, have been particularly successful in classifying natural images and have demonstrated effectiveness in medical image classification tasks [6]. For example, CNN models have played a significant role in classifying nonproliferative diabetic retinopathy (NPDR) with high sensitivity and specificity using fundus images. Additionally, they have improved the efficiency, accessibility, and affordability of diabetic retinopathy grading systems by outperforming conventional hand-designed feature-based methods when validated on large datasets in various settings. The paper starts by reviewing a wide range of literature in Section II, focusing on relevant research in the field. In Section III, the materials and methods used are outlined. Then, Section IV offers the proposed methodology used in the paper. Section V presents the results obtained from simulations conducted using MATLAB, along with a detailed analysis. Finally, Section V wraps up the paper by summarizing the findings and providing concluding remarks.

II. Literature Review

State-of-the-art automatic diabetic retinopathy (DR) detection techniques can be broadly classified into two categories. The older studies primarily utilize classical image processing techniques to detect, segment, and analyze lesions in images based on their precise characteristics. These techniques employ a series of predefined algorithms to identify specific features such as microaneurysms, hemorrhages, exudates, and blood vessels. Methods such as morphological operations, thresholding, and edge detection are commonly used for lesion detection and segmentation. In contrast, more recent studies rely on Convolutional Neural Networks (CNNs) to perform both feature extraction and classification [7]. CNNs have shown remarkable effectiveness in learning discriminative features directly from the images, thereby eliminating the need for handcrafted feature extraction. This approach offers a more holistic and datadriven solution to DR detection, potentially improving accuracy and efficiency compared to traditional image processing methods. The authors of [8] categorized diabetic retinopathy features, such as microaneurysms, hemorrhages, exudates, and blood vessels, into four groups for computer-aided diagnosis systems: optic disc localization and segmentation, exudate segmentation, blood vessel segmentation, and geometric and hemodynamic features, as well as diabetic retinopathy detection and classification. Exudates, a common feature of diabetic retinopathy, can be detected using morphological operations and Renyi entropy thresholding as proposed by the authors of [9]. This method involves three main stages: image enhancement through morphological operations, optic disc detection and removal, and exudate segmentation using Renyi entropy thresholding. Additionally, exudate segmentation has been proposed using a saliency method based on regions, which involves detecting exudates on exudate patches after optic disc removal and recombining them into a complete image. Another feature, red small dots, comprising microaneurysms and tiny hemorrhages, can be detected using the Tyler Coye algorithm and morphological operations as proposed in [10]. This process involves detecting and removing bright areas like optic discs and exudates, segmenting dark areas, performing blood vessel segmentation, and then identifying red small dots. The authors of [11] utilized objects from exudates to determine moderate and severe non-proliferative diabetic retinopathy (NPDR). Their system involves pre-processing and segmentation using morphological operations, feature extraction including area, perimeter, number of centroids, and standard deviation, and classification using soft margin Support Vector Machine (SVM). In [12], the author proposed a technique aimed at enhancing the quality of fundus images. This method involved applying morphological operations along with Contrast Limited Adaptive Histogram Equalization (CLAHE) to improve the visibility of vessels in the images. In [13], new methods of image transformations were illustrated to enhance retinal images, including wavelet transform, curvelet transform, and contourlet transform. The paper extracted various features and conducted comparisons among these three transformations.

The authors of [14] utilized Support Vector Machines (SVM) and k-Nearest Neighbors (KNN) for the classification of Diabetic Retinopathy, which yielded promising comparative results. The detection of exudates (EXs) from fundus images was achieved by leveraging core signs of DR. Specifically, Fuzzy C-Means (FCM) was employed for EX detection in [15]. Gray Level Co-occurrence Matrix (GLCM) was utilized to examine the relationship between pixel intensities in retinal images, offering insights into texture features. Histogram calculation provided information about the intensity distribution, facilitating the prediction of pixel relationships. Morphological techniques were applied for EX detection in retinal images, followed by the use of Probabilistic Neural Network (PNN) to distinguish between normal and abnormal images [16]. To identify EXs, a two-step process involving rough segmentation and fine segmentation was employed. Rough segmentation utilized morphological and column-wise operations, while fine segmentation involved morphological reconstruction [17]. Machine learning methods were proposed by many researchers to determine the presence or absence of EXs, extracting features such as centroids, means, and standard deviations [18].

Dynamic thresholding and median filtering techniques were proposed for the detection of hard EXs [19]. Both texture and wavelet features were used for classifying lesion and non-lesion regions. Bright lesions were detected using Otsu's thresholding and Sobel edge detector methods [20]. In recent years, Convolutional Neural Networks (CNNs) have made significant advancements in computer vision and image classification. Several studies have utilized CNNs to classify diabetic retinopathy. For example, the authors of [21] enhanced input images and employed CNN architectures such as

REDVET - Revista electrónica de Veterinaria - ISSN 1695-7504
Vol 24, No.4 (2023) http://www.veterinaria.org
Article Received: September 2023; Revised: October 2023; Published: November 2023

AlexNet, VGGNet, GoogLeNet, and ResNet through transfer learning. While CNNs can perform feature extraction and classification simultaneously, fine-tuning CNNs for classification may require longer computation times.

III. Materials And Methods

3.1 CNN-based Deep Features

The advent of deep learning has revolutionized computer vision, facilitating the automatic extraction of complex and abstract image representations. Among the myriad deep learning architectures, Convolutional Neural Networks (CNNs) have emerged as a cornerstone, particularly renowned for their prowess in feature extraction and representation learning. In the approach delineated in this dissertation, a pre-trained CNN architecture is leveraged to extract deep features from input images. These deep features are meticulously engineered to encapsulate both low-level and highlevel image attributes, endowing the methodology with the capability to discern between authentic and manipulated regions effectively.

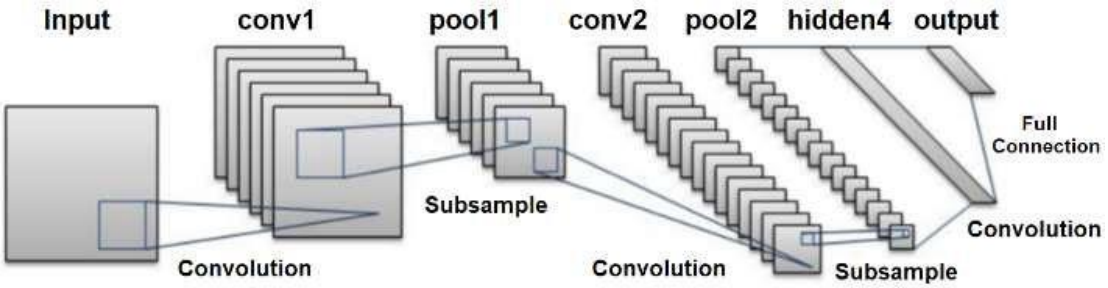

Figure 1: Schematic Depiction of a Deep Convolutional Neural Network [21]

The Convolution Operation: At its essence, convolution entails the integration of two functions, typically involving real numbers as variables. Mathematically, the convolution operation is formally defined as:

$$s(t) = \int x(a)w(t-a)da \quad (1)$$

In CNN, this operation is often succinctly expressed as:

$$s(t) = (x * w)(t) \quad (2)$$

Here, the first function (x) denotes the input, while the second function (w) represents the kernel. The result of this convolution operation is termed a feature map. When working with discrete data in computational contexts, continuous functions are approximated as a sum of "discrete" functions, taking the form:

$$S(t) = (x * w)(t) = \sum^{\infty}_{a=-\infty} x(a)w(t-a) \quad (3)$$

In the domain of deep learning, the input typically comprises a multi-dimensional vector (tensor), whereas the kernel is often a multi-dimensional parameter vector adjusted during the learning process. For instance, when utilizing an image (I) as input data, a two-dimensional kernel (K) is commonly employed, denoted as:

$$S(i,j) = (I * K)(i,j) = \sum_m \sum_n I(i-m, j-n)K(m,n) \quad (4)$$

3.2 Gray-Level Co-occurrence Matrix (GLCM)

The GLCM, symbolized as $P(i, j|d, \theta)$, signifies the joint probability of encountering two pixels with intensity values i and j at a given relative displacement d and angle θ within the image. Computation of GLCM involves traversing a window of predetermined size across the image and tallying the occurrences of pixel pairs adhering to the displacement and angle criteria. Mathematically, it is represented as:

$P(i, j|d, \theta) = \sum_x \sum_y \delta(I(x, y) - i)\delta(I(x + d\cos(\theta), y + d\sin(\theta) - j)$ (5) **Here:**

- $P(i, j|d, \theta)$ denotes the GLCM at displacement d and angle θ for pixel values i and j.
- δ stands for the Kronecker delta function, yielding 1 if the condition inside holds true and 0 otherwise.
- $I(x, y)$ represents the pixel value at position (x, y) in the image.
- d corresponds to the displacement (i.e., the spatial gap between two pixels).
- θ denotes the angle under consideration for co-occurrence analysis, conventionally set at 0°, 45°, 90°, and 135°.

REDVET - Revista electrónica de Veterinaria - ISSN 1695-7504
Vol 24, No.4 (2023) http://www.veterinaria.org
Article Received: September 2023; Revised: October 2023; Published: November 2023

3.2.1 Normalization of GLCM

Normalization of GLCM is imperative to confine its values within the range of [0, 1], thereby rendering the features insensitive to alterations in image contrast and brightness. Typically, normalization entails dividing the GLCM by the summation of all its elements, as depicted by the equation:

$$P_{normalized}(i, j|d, \theta) = \frac{P(i,j|d,\theta)}{\sum_i \sum_j P(i,j|d,\theta)} \quad (6)$$

3.2.2 Computation of GLCM Features

Post normalization, diverse texture features can be derived from the GLCM. These features serve as descriptors of textural properties within the image. Prominent GLCM features include:

Contrast: Signifying the local fluctuations in pixel intensity values, it is calculated as:

$$Contrast = \sum_i \sum_j (i-j)^2 P_{normalized}(i, j|d, \theta) \quad (7)$$

Energy (Angular Second Moment): Reflecting the uniformity or homogeneity of texture, it is computed as:

$$Energy = \sum_i \sum_j [P_{normalized}(i, j|d, \theta)]^2 \quad (8)$$

Entropy: Capturing the randomness or complexity inherent in the texture, it is expressed as:

$$Entropy = -\sum_i \sum_j P_{normalized}(i, j|d, \theta) \log[P_{normalized}(i, j|d, \theta)] \quad (9)$$

Correlation: Describing the linear interdependence between pixel pairs, it is given by:

$$Correlation = \frac{\sum_i \sum_j (i-\mu)(j-\nu) P_{normalized}(i, j|d, \theta)}{\sigma_i \sigma_j} \quad (10)$$

Here:

- μ and ν represent the means of the marginal distributions of i and j, respectively.
- σ_i and σ_j denote the standard deviations of the marginal distributions of i and j, respectively.

GLCM-based texture feature extraction serves as a pivotal tool in characterizing the underlying textural intricacies within images, facilitating diverse applications across domains ranging from medical imaging to remote sensing.

IV. PROPOSED METHODOLOGY

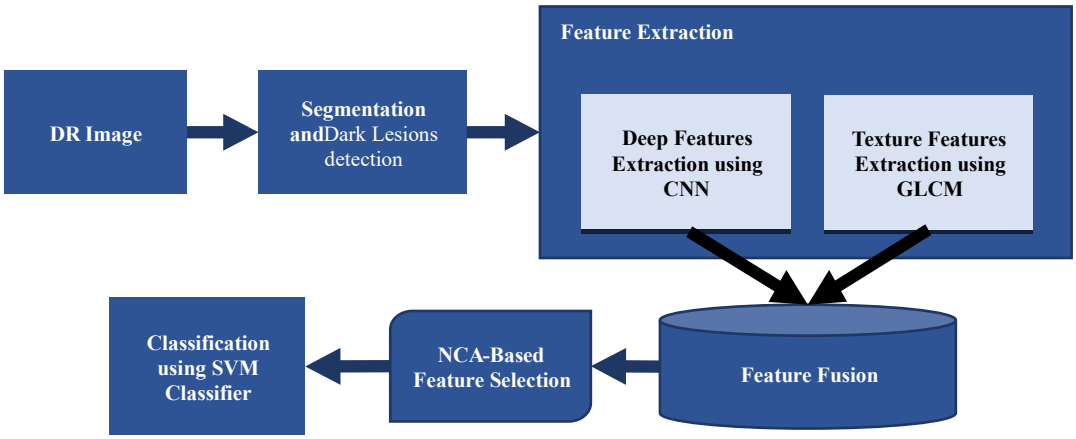

Figure 2: Schematic Representation of the Proposed Methodology for DR Detection

4.1 Image Pre-Processing

Pre-Processing: In order to improve the image quality, we work on the green channel of the RGB color space, then we apply an adaptive histogram equalization on this channel. Additionally, to remove clear lesions if they are close to hemorrhages, we apply a morphological aperture on the enhanced image. The size of the structuring element must not be

REDVET - Revista electrónica de Veterinaria - ISSN 1695-7504
Vol 24, No.4 (2023) http://www.veterinaria.org
Article Received: September 2023; Revised: October 2023; Published: November 2023

higher, otherwise the hemorrhages will present discontinuities (Figure 3(b)). Finally, the noises are minimized by the application of a small size Gaussian filter.

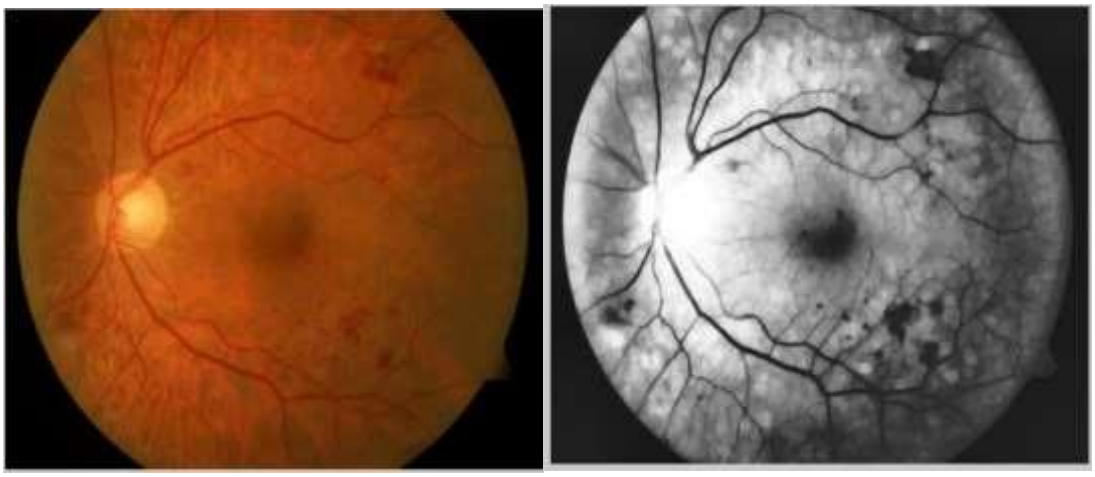

(a) **(b)**

Figure 3: Preprocessing of the original image; (a): original image; (b): enhanced image

Detection of Dark (Red) Regions: Knowing that the pixel values of hemorrhages are lower than those of other regions such as the vascular network, the macula, the micro-aneurysms, we perform the following steps to detect these regions:

- The first step was to apply a median filter of masks of 6×6 pixels and 130×130 pixels Then, a subtraction operation between these two images.
- The second step is to apply a thresholding operation (Figure 4).

$$IMF_1 = Ts[IMF_{d(6\times6)} - IMF_{d(130\times130)}] \qquad (11)$$

Where, IMF_1:dark regions in the image; Ts: image thresholding; $IMF_{d(6\times6)}$: the median filter of size 6×6; $IMF_{d(130\times130)}$: median filter of size 130×130.

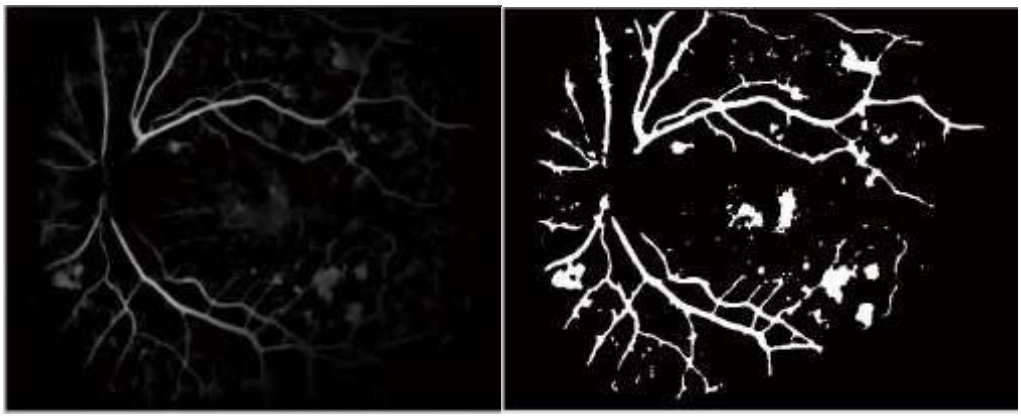

(a) **(b)**

Figure 4: Detection of red candidate regions; (a): Results of extraction of red regions; (b): result of thresholding on the smoothed image

Extraction of Red Regions: The extraction of the red structures is accomplished by the use of the black top hat transformation. This transformation makes it possible to bring out all the objects which cannot contain a structuring element of size $'b'$, as is the case for small objects (micro-aneurysms), but also for objects of elongated shape (vascular network).

$$ch(f)_\emptyset = \emptyset(f) - f \qquad (12)$$

Where, $ch(f)_\emptyset$ is the image of the black top hat; $\emptyset(f)$ is the morphological closure of the improved image; f is the improved image.

4.2 CNN-based Deep Features Extraction

The process of extracting CNN-based deep features involves configuring a CNN architecture to capture pertinent patterns and information specific to the task at hand.The Common options include VGG, ResNet, Inception, or even custom-designed architectures. Factors influencing the choice include the complexity of lesion patterns, the availability of pre-trained models, and computational resources.Input preprocessing plays a crucial role in preparing images for the CNN model. This typically involves resizing images to a standardized resolution, normalizing pixel values, and applying augmentation techniques such as rotations and flips to enhance the model's robustness.Leveraging pre-trained CNN models trained on large-scale image datasets like ImageNet can expedite the training process and potentially improve overall performance. Fine-tuning these pre-trained models involves adjusting the top layers to align with the specific output requirements of the problem at hand.In CNN-based feature extraction, the process entails passing input images through the network and extracting features from one or more intermediate layers. These extracted features encapsulate hierarchical information, ranging from low-level textures to high-level semantic content.

4.2.1 Mathematical Formulation

The essential components can be defined mathematically as follows:

CNN Model: Represented as a function f_{CNN}, the CNN model takes an input image I and generates feature maps at a specific layer L:

$$F_L = f_{CNN}(I) \tag{13}$$

Here, F_L denotes the set of feature maps at layer L, and I represents the input image.

Feature Extraction: The extraction process involves selecting one or more feature maps from layer L to represent the input image. These feature maps are then flattened into a vector, resulting in the extracted deep features:

$$F_{extracted} = Flatten(F_L) \tag{14}$$

Here, $F_{extracted}$ represents the vector of extracted deep features.

4.3 Texture Features Extraction using GLCM

Texture features extraction using GLCM involves analyzing the frequency of occurrence of pairs of pixel intensities within a defined neighborhood in an image. This method aims to quantify the frequency of different pairs of gray levels appearing together at a specific distance and orientation within the image, thereby capturing textural information encompassing patterns, structures, and variations. The mathematical foundation of GLCM features extraction is previously explained in section 3.2.

4.4 Combining Deep Features and GLCM Features

Combining deep features from CNN with GLCM features presents a robust strategy for enhancing image analysis tasks, such as diabetic retinopathy detection. This approach aims to harness both the textural insights provided by GLCM and the semantic knowledge embedded in deep features to bolster the efficacy of the detection system.

4.4.1 Feature Fusion Process

The amalgamation of deep features and GLCM features entails consolidating these distinct sets of descriptors into a unified feature vector. The sequential steps involved in this process are delineated as follows:

Deep Feature Extraction:Deep features are extracted from input images using either a pretrained CNN model or a bespoke architecture tailored to the specific task at hand.
These deep features encapsulate high-level semantic representations discerned from the images by the CNN.

GLCM Feature Extraction:GLCM features are computed by scrutinizing the spatial relationships among pixel values, thereby encapsulating textural nuances within the images.
It's common practice to compute multiple GLCMs corresponding to diverse orientations and displacements.

Feature Fusion:Extracted deep features and GLCM features are melded together through concatenation or another fusion mechanism to construct a hybrid feature vector.

Concatenation emerges as a prevalent approach, yielding a feature vector comprising deep features followed by GLCM features.

4.4.2 Mathematical Formulation of Feature Fusion

Let D signify the deep features procured from the CNN, and G denote the GLCM features. The resultant combined feature vector F can be mathematically expressed as:

$$F = [D, G] \quad (15)$$

Here, $[D, G]$ signifies the concatenation of deep features D and GLCM features G into a cohesive vector. This integrated feature representation amalgamates the complementary insights furnished by both deep learning-based semantic analysis and texture-based GLCM analysis, thereby furnishing a comprehensive characterization of image content suitable for a diverse array of applications.

4.5 NCA-Based Feature Selection

Neighborhood Component Analysis (NCA) offers a dimensionality reduction avenue, strategically curating a subset of features to heighten the efficacy of classification or clustering tasks. Within the realm of amalgamated deep and GLCM features, NCA emerges as a potent tool for discerning the most salient features from the hybrid feature vector.

4.5.1 Objective Function Formulation

The core of NCA lies in maximizing a stochastic objective function, gauging the efficacy of feature selection regarding the task's objectives. This objective function is mathematically articulated as:

$$J(f) = \sum_{i=1}^{N} p_i \sum_{j \neq i} p_j 1(y_i = y_j)\ exp\ (-\|f(x_i) - f(x_j)\|^2) \quad (16)$$

Here's a breakdown:

- f symbolizes the feature selection function.
- x_i and x_j denote data samples, while y_i and y_j represent their corresponding labels.
- $1(y_i = y_i)$ acts as an indicator function, assuming a value of 1 if $y_i = y_j$ (indicating samples from the same class) and 0 otherwise.
- p_i signifies the probability of selecting sample x_i for optimization.

4.5.2 Optimization Strategies

NCA harnesses optimization methodologies like stochastic gradient descent (SGD) to ascertain the optimal feature selection function f that maximizes the objective function $J(f)$. Through iterative updates, the feature selection mechanism evolves in alignment with the overarching task objectives.

4.5.3 Feature Selection Outcome

The culmination of the NCA-driven optimization endeavor yields a subset of the combined feature vector F, comprising the most discerning features as per the NCA criterion. These handpicked features epitomize the information relevant to the classification task, setting the stage for subsequent processing endeavors such as diabetic retinopathy detection.

4.6 Classification using Support Vector Machine

In the realm of classification algorithms, SVM stands as a stalwart, proficient in discerning patterns indicative of diabetic retinopathy within retinal images. In the pursuit of accurately identifying signs of diabetic retinopathy, SVM assumes a pivotal role, leveraging features meticulously selected through NCA.

4.6.1 SVM Formulation

At the heart of SVM lies the formulation aimed at tackling binary classification predicaments. This formulation unfolds against the backdrop of a training dataset depicted as:

$$TrainingDataset = \{(x_1, y_1), (x_2, y_2), \dots, (x_N, y_N)\} \quad (17)$$

Here:

- x_i embodies a feature vector, comprising NCA-selected features, delineated across a dimensionality of dd for the i^{th} sample.

REDVET - Revista electrónica de Veterinaria - ISSN 1695-7504
Vol 24, No.4 (2023) http://www.veterinaria.org
Article Received: September 2023; Revised: October 2023; Published: November 2023

• y_i symbolizes the corresponding class label, with $y_i \in \{-1, +1\}$ denoting authenticity (-1) or lesion$(+1)$.
SVM endeavors to carve out a hyperplane characterized by a weight vector w and a bias term b, effectively segregating the data points. The decision function is articulated as:

$$f(x) = sign(w \cdot x + b) \quad (18)$$

Where:
• $f(x)$ assumes the mantle of the decision function, orchestrating the prediction of the class label for a given input feature vector x.
• w embodies the weight vector.
• b denotes the bias term.
• The dot product $(\cdot)$ orchestrates the mathematical interplay.
Pseudo Code for diabetic retinopathy with SVM and NCA-Selected Features
Step 1: Feature Extraction and Selection
Extract features from images using CNN and GLCM.
Select the most informative features using NCA-based feature selection.
Step 2: Data Preparation
Split the dataset into training and testing sets.
Encode class labels (e.g., -1 for authentic, +1 for lesion).
Step 3: SVM Training
Train an SVM classifier on the training data with NCA-selected features.
Choose appropriate SVM parameters (e.g., C and kernel type).
Step 4: SVM Testing
Use the trained SVM model to predict class labels for the testing data.
Step 5: Performance Evaluation
Evaluate the classification performance using metrics like accuracy, precision, recall, and F1-score.
Step 6: Interpretation and Reporting
Examine the results to identify diabetic retinopathy in the tested images. Report the locations and characteristics of detected lesion.

V. Simulation Results and Discussion

5.1 Database

Image databases are an essential resource in the development of retinal image analysis algorithms, they greatly help researchers to evaluate and compare the methods developed with the work reported in the state of the art. They lead to the development of better algorithms. In this section, we present the different databases used in our work.

5.1.1 DRIVE Image Database

The Drive image database includes 40 color fundus images, 7 of which show pathologies. Images are acquired with a non-mydriatic retinograph (Canon RC5) with a 45-degree field of view (FOV). They are saved in JPEG format, with a size of 768×584 pixels. The image base is divided into two sets (20 images for training and the rest for testing). Manual segmentation of the vascular network is performed by two experienced ophthalmologists.

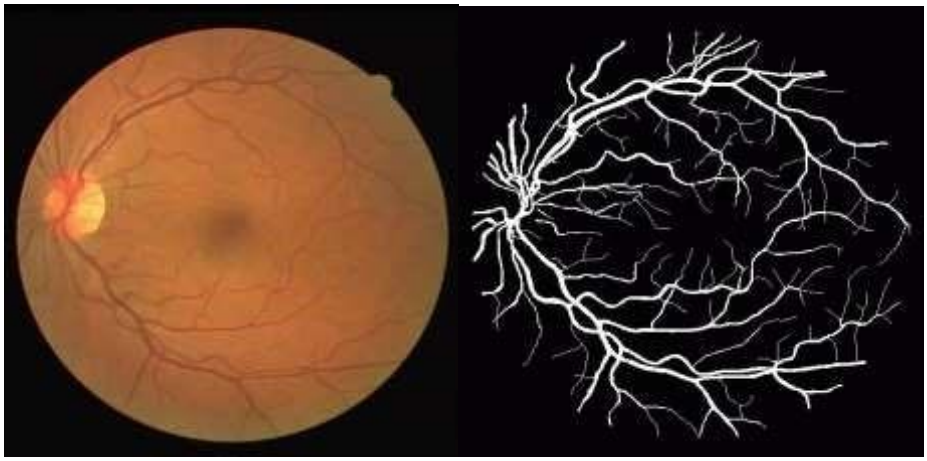

REDVET - Revista electrónica de Veterinaria - ISSN 1695-7504
Vol 24, No.4 (2023) http://www.veterinaria.org
Article Received: September 2023; Revised: October 2023; Published: November 2023

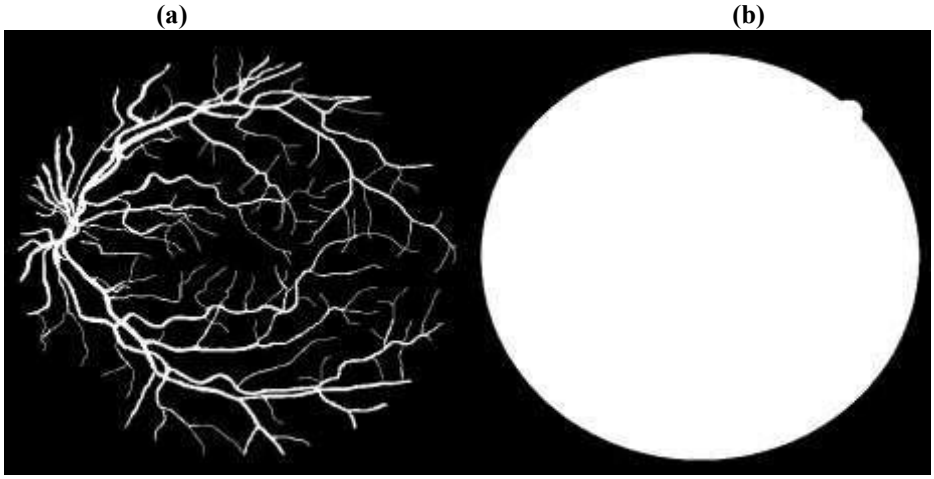

Figure 5: Sample images from the DRIVE database; (a): original image; (b): manual segmentation of the vascular network by the first ophthalmologist (c): manual segmentation of the vascular network by a second ophthalmologist; (d): mask of the original image

5.1.2 Fundus Image

This dataset, Fundus Image Registration Dataset (also known as FIRE) consists of 129 retinal images forming 134 image pairs. These image pairs are split into 3 different categories depending on their characteristics. The images were acquired with a Nidek AFC-210 fundus camera, which acquires images with a resolution of 2912×2912 pixels and a FOV of 45° both in the x and y dimensions. Images were acquired at the Papageorgiou Hospital, Aristotle University of Thessaloniki, Thessaloniki from 39 patients.

5.2 Evaluation Parameters

Table 1: Evaluation Parameters

TP (True Positive)	"Represents the count of dark lesions in retinal images correctly detected"
TN (True Negative)	"Indicates the number of regions correctly identified as not containing dark lesions in retinal images."
FP (False Positive)	"Represents the number of regions incorrectly identified as containing dark lesions in retinal images when they do not."
FN (False Negative)	"Indicates the number of dark lesions in retinal images that were missed or incorrectly identified as not present."

$$Accuracy = \frac{TP + TN}{TP + TN + FP + FN} \quad (19)$$

$$Precision = \frac{TP}{TP + FP} \quad (20)$$

$$Sensitivity = \frac{TP}{TP + FN} \quad (21)$$

$$Specificity = \frac{TN}{TN + FN} \quad (22)$$

REDVET - Revista electrónica de Veterinaria - ISSN 1695-7504
Vol 24, No.4 (2023) http://www.veterinaria.org
Article Received: September 2023; Revised: October 2023; Published: November 2023

$$ErrorRate = \frac{FP + FN}{TP + TN + FP + FN} \quad (23)$$

$$FalsePositiveRate(FPR) = \frac{FP}{FP + TN} \quad (24)$$

$$F - Score = \frac{2TP}{2TP + FP + FN} \quad (25)$$

5.3 Results

5.3.1 Detection of Dark Lesions in Retinal Images

As the number of patients with diabetes is increasing, therefore, early detection of diabetic retinopathy for regular screening can prevent vision loss and blindness. Indeed, the development of algorithms for the detection of dark lesions characteristic of DR (blood and micro-aneurysms) helps ophthalmologists to make the decision whether the suspicious signs of DR are present or not in the image to a computer-assisted mass screening system.

Pre-Processing: Knowing that the illumination in the central regions relative to the edge of the image is not uniform and that the red (dark) elements appear with the strongest contrast in the green channel of the RGB color space, we work on this channel. Subsequently, an adaptive histogram equalization is applied to the green channel. In addition, the noise present in the image is eliminated by applying a median filter (Figure 6(a)).

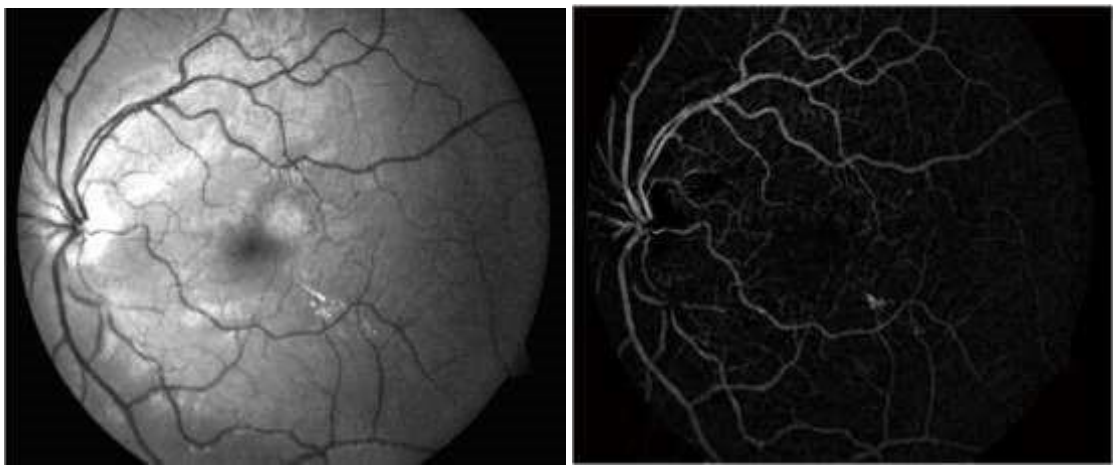

(a) **(b)**

Figure 6: Extraction of red regions. (a) improved image; (b): The top hat of the enhanced image

Extracting the Candidate Region: To extract the microaneurysm candidates we apply a thresholding operation on the top hat result with a threshold ($58 \leq T \leq 155$) because after several trials we found that this threshold gives good results with decrease false positive.

As a result, knowing that the micro-aneurysms appear in the form of tiny dots, we remove from the resulting binary image the small objects or pixels of size 10 and pixels of size 100 after, a subtraction is performed between these last two operations, results is shown in Figure 7.

REDVET - Revista electrónica de Veterinaria - ISSN 1695-7504
Vol 24, No.4 (2023) http://www.veterinaria.org
Article Received: September 2023; Revised: October 2023; Published: November 2023

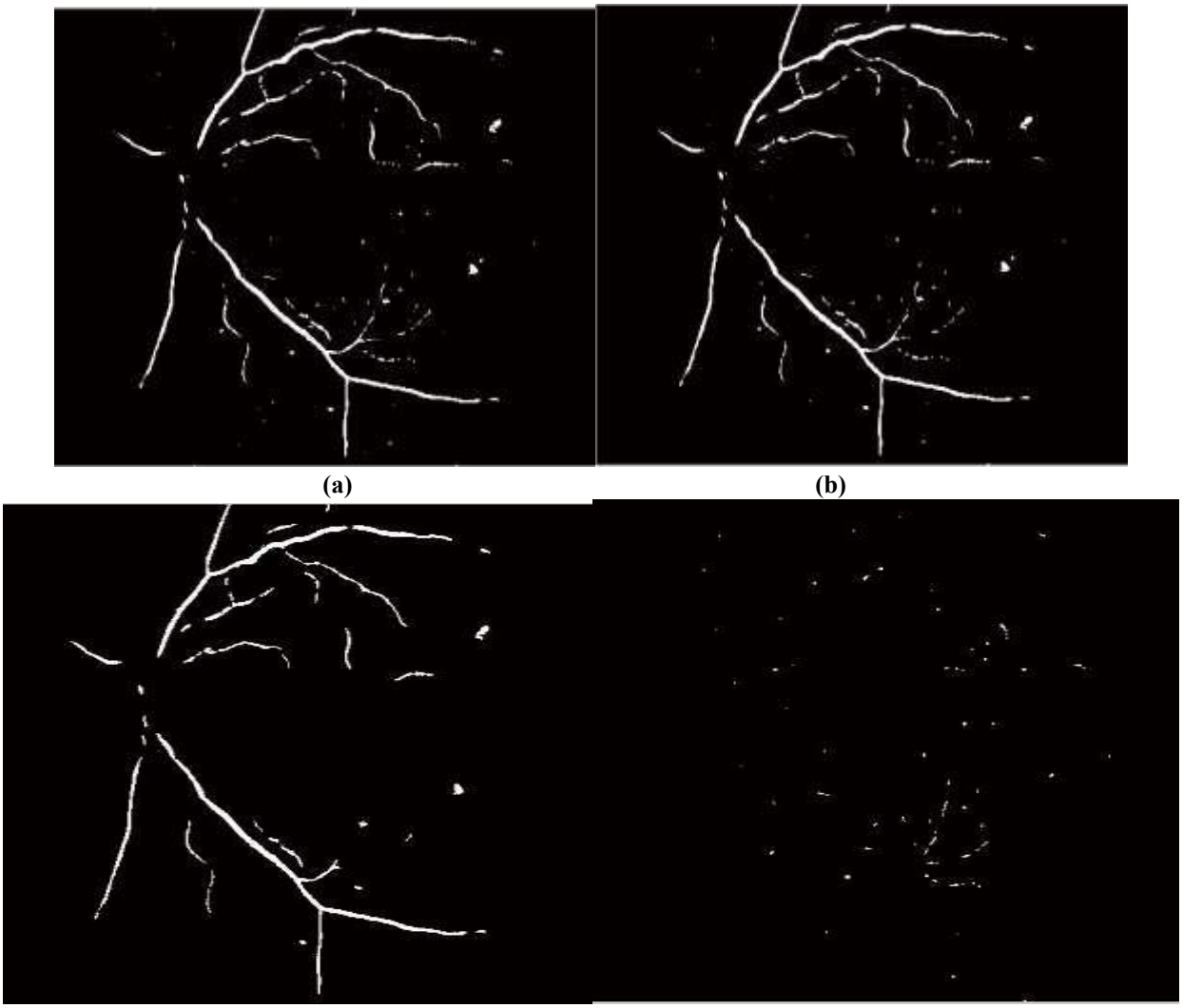

(a) **(b)**

(b) **(d)**

Figure 7: Candidate extraction (a) thresholding operation of the top hat image; (b) removing the objects from (10); (c) removal of objects from (100); (d) subtraction operation

After the subtraction operation between the results of the elimination of pixels from 10 to 100, we notice that the vascular network has been eliminated, but there remains some segment of vessels that are considered noise. Segmentation and Elimination of the Vascular Network:

Since the candidate extraction result (Figure 7(d)) represents the small vessels and some particles belong to the vascular networks which are considered as noise, it is therefore preferable to extract the vascular network to eliminate these noises.

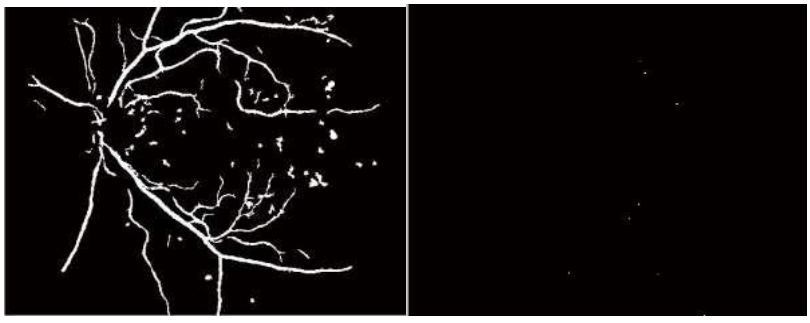

(a) **b)**

Figure 8: Segmentation and elimination of the vascular network; a) Extraction of the vascular network; b) elimination of vascular network

REDVET - Revista electrónica de Veterinaria - ISSN 1695-7504
Vol 24, No.4 (2023) http://www.veterinaria.org
Article Received: September 2023; Revised: October 2023; Published: November 2023

As the vascular network belongs to the red regions like the micro-aneurysms, it appears in the result of the top hat, indeed; to extract the latter and separate it from the microaneurysms, we apply automatic thresholding to the image of the top hat (Figure 8(a)).

In order to eliminate continuities and segments of vascular network which represents a false positive in candidate extraction result, we use a for loop in which we add the size of segmented vascular network and subtraction results (Figure 7(d)). Final result is shown in the Figure 9.

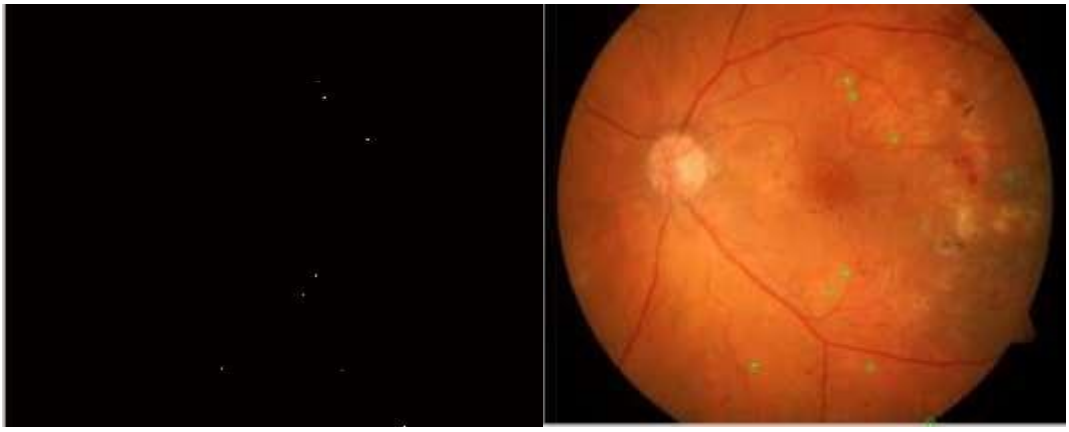

(a) **(b)**

Figure 9: Final result for the detection of micro-aneurysms; (a) detection of micro aneurysms and elimination of false positives; (b) overlay on the original image

The proposed method was tested on several images from different databases containing different image quality with several lesions such as hemorrhages and exudates. It can be seen that the micro-aneurysms have been well identified. They correspond to manual detection by ophthalmologists, the results were satisfactory in good quality images. In cases where the micro-aneurysms appear with low contrast or in dark images the results were acceptable. In addition, in the case where the images containing large hemorrhages, the results obtained were satisfactory, the algorithm is sensitive to the noise caused by the acquisition system. Here is some examples in Figure 10.

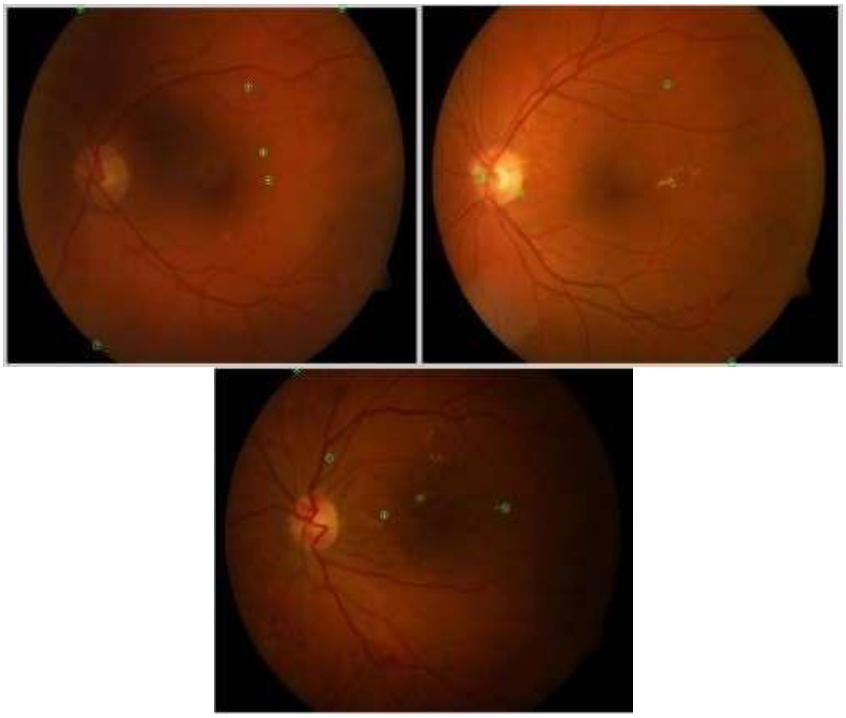

Figure 10: Example for detection of micro-aneurysms

REDVET - Revista electrónica de Veterinaria - ISSN 1695-7504
Vol 24, No.4 (2023) http://www.veterinaria.org
Article Received: September 2023; Revised: October 2023; Published: November 2023

5.3.2 Hemorrhage Detection in Color Images of the Retina

Hemorrhages are red spots, which are important in predicting the severity of NPDR. The problem in detecting hemorrhages is lack of information: variable size and shape, contrast can be weak or strong, color- although red varies from image to image. Indeed, the majority of work developed in this field detects in agiographic images which hemorrhages appear with strong contrast (Figure 11).

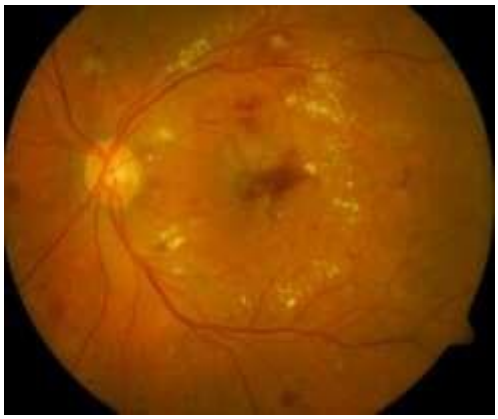

Figure 11: Example of the presence of haemorrhages shown by a circle

The proposed hemorrhage detection algorithm was tested on a series of images from the DiaretDB1 and DiaretDB0 databases. These bases were chosen in relation to other existing bases because the different lesions: haemorrhages, micro-aneurysms, hard and soft exudates are marked by experts. All large hemorrhages were successfully identified. However, in a few images, the algorithm missed a few hemorrhages that were small, low-contrast or located in the center of the macula or connected to the vascular network. These undetected hemorrhageswere eliminated with the macula or the vascular network. Clinically, ophthalmologists are not interested in small hemorrhages. Examples of hemorrhage detection are shown in Figure 12.

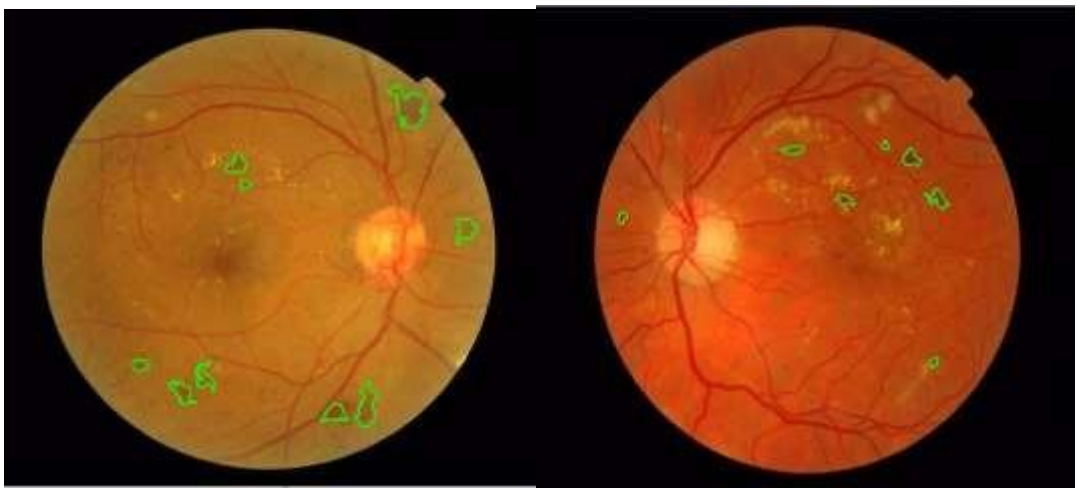

Figure 12: Examples of haemorrhage detection

Table 2: Comparative results of Different dataset using SVM classifier

Parameters	**MESSIDOR**	**DRIVE**	**STARE**
Accuracy	0.9907	0.9583	0.9722
Error Rate	0.0093	0.0417	0.0278
Sensitivity	0.9917	0.9583	0.9722
Specificity	0.9968	0.9861	0.9907
Precision	0.9917	0.9623	0.975
False Positive Rate	0.0032	0.0139	0.0093
F-Score	0.9915	0.9586	0.9721

MCC	0.9885	0.9462	0.9642
Kappa Statistics	0.9753	0.8889	0.9259

Table 3: Comparative results of Different dataset using different features in SVM classifiers

Parameters	GLCM	CNN	Hybrid
Accuracy	0.975	0.9853	0.9907
Error Rate	0.025	0.0147	0.0093
Sensitivity	0.975	0.9853	0.9917
Specificity	0.9917	0.9951	0.9968
Precision	0.9753	0.9861	0.9917
False Positive Rate	0.0083	0.0049	0.0032
F-Score	0.9749	0.9853	0.9915
MCC	0.9668	0.9808	0.9885
Kappa Statistics	0.9333	0.9608	0.9753

The provided table presents the performance metrics of three different classification algorithms (not specified) on three different datasets: MESSIDOR, DRIVE, and STARE. Here is a brief analysis of the results:
Accuracy: Accuracy measures the proportion of correctly classified instances over the total number of instances. The algorithms achieve high accuracy scores across all three datasets, ranging from 0.917 to 0.981. MESSIDOR has the highest accuracy (0.981), followed by STARE (0.963) and DRIVE (0.917).
Error Rate: The error rate is the complement of accuracy and represents the proportion of misclassified instances. Lower error rates indicate better performance. The algorithms achieve relatively low error rates, ranging from 0.0185 to 0.0833. MESSIDOR has the lowest error rate (0.0185), followed by STARE (0.037) and DRIVE (0.0833).
Sensitivity: Sensitivity, also known as the true positive rate or recall, measures the proportion of correctly classified positive instances (e.g., presence of a condition) out of all actual positive instances. The algorithms achieve perfect sensitivity scores (1.0) on MESSIDOR and DRIVE datasets, while STARE achieves a sensitivity of 1.0.
Specificity: Specificity measures the proportion of correctly classified negative instances (e.g., absence of a condition) out of all actual negative instances. The algorithms achieve specificities ranging from 0.833 to 0.963. DRIVE has the lowest specificity (0.833), while MESSIDOR has the highest (0.963), and STARE falls in between (0.926). Precision: Precision calculates the proportion of correctly classified positive instances out of all instances predicted as positive. It reflects the accuracy of positive predictions. The algorithms achieve precision scores ranging from 0.857 to 0.964. MESSIDOR has the highest precision (0.964), followed by STARE (0.931) and DRIVE (0.857). False Positive Rate: The false positive rate measures the proportion of negative instances that are incorrectly classified as positive. Lower false positive rates indicate better performance. The algorithms achieve false positive rates ranging from 0.037 to 0.167. MESSIDOR has the lowest false positive rate (0.037), while DRIVE has the highest (0.167), and STARE falls in between (0.074). F-Score: The F-Score, or F1-Score, is the harmonic mean of precision and recall. It provides a balanced measure of a classifier's performance on both positive and negative instances. The algorithms achieve high F-Scores ranging from 0.923 to 0.982. MESSIDOR has the highest F-Score (0.982), followed by STARE (0.964) and DRIVE (0.923).
The algorithms exhibit strong performance on all three datasets, achieving high accuracy, sensitivity, and precision, while maintaining low error rates and false positive rates. MESSIDOR generally performs the best across most metrics, followed by STARE, while DRIVE shows slightly lower performance. The choice of the most suitable algorithm would depend on the specific requirements of the classification task and the trade-offs between different performance metrics.

Table 4: Comparative results of different classifiers on Drive dataset

Parameters	SVM (Proposed)	KNN [14]	RF [22]
Accuracy	0.9907	0.9444	0.9667
Error Rate	0.0093	0.0556	0.0333
Sensitivity	0.9917	0.9444	0.9667
Specificity	0.9968	0.9815	0.9889
Precision	0.9917	0.9545	0.9682
False Positive Rate	0.0032	0.0185	0.0111
F-Score	0.9915	0.9456	0.9669
MCC	0.9885	0.9305	0.9562
Kappa Statistics	0.9753	0.8519	0.9111

Table 4 presents a comprehensive comparison of the performance of different classifiers, namely proposed Support Vector Machine (SVM), k-Nearest Neighbors (KNN) [14], and Random Forest (RF) [22], based on various evaluation parameters using the DRIVE dataset. These parameters include accuracy, error rate, sensitivity, specificity, precision, false positive rate, F-Score, Matthews Correlation Coefficient (MCC), and Kappa statistics. The results indicate that the proposed SVM model achieves the highest accuracy (99.07%), sensitivity, specificity, precision, F-Score, MCC, and Kappa statistics compared to KNN and RF. Notably, the false positive rate is significantly lower for the proposed SVM model compared to KNN and RF, showcasing its effectiveness in minimizing misclassifications. This suggests that the proposed SVM model is superior in classifying retinal images for the detection of dark lesions, as supported by the provided citation references [14][22].

VI. Conclusion

This paper endeavors to automate the detection and classification of diabetic retinopathy from retinal fundus images, a critical task in ophthalmology. While previous methods have relied on handcrafted features and manually designed convolutional neural network (CNN) architectures for classification, this paper introduces a novel approach that integrates deep learning techniques with texture analysis to enhance detection accuracy. By combining CNN-based deep features extraction with Gray-Level Co-occurrence Matrix (GLCM) texture features extraction and employing a feature fusion process along with Neighborhood Component Analysis (NCA)-based feature selection, the proposed methodology aims to optimize feature representation. The classification stage utilizes Support Vector Machine (SVM) to classify retinal images based on the extracted features. Results obtained from the DRIVE dataset demonstrate the effectiveness of the proposed methodology, achieving an accuracy of 99.07% and outperforming previous research works. The results reveal that the proposed SVM model exhibits superior performance in detecting dark lesions compared to k-Nearest Neighbors (KNN) and Random Forest (RF) classifiers. Additionally, the comparative analysis across various evaluation parameters emphasizes the robustness and effectiveness of the proposed SVM model. Furthermore, detailed examinations of the detection of dark lesions and hemorrhages in retinal images elucidate the methodology's capability to accurately identify these critical indicators of diabetic retinopathy, thus highlighting its potential in aiding ophthalmologists in diagnosis and treatment decisions. Overall, this research signifies a significant advancement in automated retinal image analysis, promising improved early detection and management of diabetic retinopathy.A potential future direction could involve exploring the integration of advanced deep learning techniques, such as attention mechanisms or generative adversarial networks, to further enhance the robustness and accuracy of retinal lesion detection, especially in challenging scenarios with low contrast or complex image backgrounds.

References

1. Agarwal, S. and Bhat, A., 2023. A survey on recent developments in diabetic retinopathy detection through integration of deep learning. *Multimedia Tools and Applications*, *82*(11), pp.17321-17351.
2. Tassew, W.C., Birhan, N. and Zewdu, Y., 2023. Incidence and Predictors of Diabetic Retinopathy among Newly Diagnosed Type 2 Diabetic Patients at Chronic Follow-Up Clinic of University of Gondar Specialized Hospital: A Retrospective Follow-Up Study. *Int J Diabetes Clin Res*, *10*, p.169.
3. Tan, T.E. and Wong, T.Y., 2023. Diabetic retinopathy: Looking forward to 2030. *Frontiers in Endocrinology*, *13*, p.1077669.
4. Curran, K., Piyasena, P., Congdon, N., Duke, L., Malanda, B. and Peto, T., 2023. Inclusion of diabetic retinopathy screening strategies in national-level diabetes care planning in low-and middle-income countries: a scoping review. *Health Research Policy and Systems*, *21*(1), p.2.
5. Currie, C.J., 2024. The descriptive epidemiology of type 2 diabetes in the United Kingdom from 2004 to 2021. *medRxiv*, pp.2024-03.
6. Özbay, E., 2023. An active deep learning method for diabetic retinopathy detection in segmented fundus images using artificial bee colony algorithm. *Artificial Intelligence Review*, *56*(4), pp.3291-3318.
7. Vij, R. and Arora, S., 2023. A systematic review on diabetic retinopathy detection using deep learning techniques. *Archives of Computational Methods in Engineering*, *30*(3), pp.2211-2256.
8. Nadeem, M.W., Goh, H.G., Hussain, M., Liew, S.Y., Andonovic, I. and Khan, M.A., 2022. Deep learning for diabetic retinopathy analysis: A review, research challenges, and future directions. *Sensors*, *22*(18), p.6780.
9. Qomariah, D.U.N. and Tjandrasa, H., 2022, October. Exudate detection in retinal fundus images using combination of mathematical morphology and Renyi entropy thresholding. In *2022 11th International Conference on Information & Communication Technology and System (ICTS)* (pp. 31-36). IEEE.
10. Qomariah, D.U.N., Tjandrasa, H. and Fatichah, C., 2023, July. Classification of diabetic retinopathy and normal retinal images using CNN and SVM. In *2023 12th International Conference on Information & Communication Technology and System (ICTS)* (pp. 152-157). IEEE.

11. Putra, R.E., Tjandrasa, H., Suciati, N. and Wicaksono, A.Y., 2022, October. Non-proliferative diabetic retinopathy classification based on hard exudates using combination of frcnn, morphology, and anfis. In *2022 Third international conference on vocational education and electrical engineering (ICVEE)* (pp. 1-6). IEEE.
12. Sahu, S., Singh, A.K., Ghrera, S.P. and Elhoseny, M., 2023. An approach for de-noising and contrast enhancement of retinal fundus image using CLAHE. *Optics & Laser Technology*, *110*, pp.87-98.
13. Solhi, M., Yazdi, M. and Sharzehei, M., 2022. Fusion of Synthetic Aperture Radar Images and Optical Images Using Curvelet Transform and Retina model. *Journal of Radar and Optical Remote Sensing and GIS*, *3*(2), pp.3452.
14. Rehman, A., Harouni, M., Karimi, M., Saba, T., Bahaj, S.A. and Awan, M.J., 2022. Microscopic retinal blood vessels detection and segmentation using support vector machine and K-nearest neighbors. *Microscopy research and technique*, *85*(5), pp.1899-1914.
15. Asiri, N., Hussain, M., Adel, F.A. and Aboalsamh, H., 2021. A deep learning-based unified framework for red lesions detection on retinal fundus images. *arXiv preprint arXiv:2109.05021*.
16. Bhardwaj, C., Jain, S. and Sood, M., 2023. Diabetic retinopathy lesion discriminative diagnostic system for retinal fundus images. *Advanced Biomedical Engineering*, *9*, pp.71-82.
17. Javidi, M., Harati, A. and Pourreza, H., 2021. Retinal image assessment using bi-level adaptive morphological component analysis. *Artificial intelligence in medicine*, *99*, p.101702.
18. Das, S. and Majumder, S., 2022. Overview and Analysis of Present-Day Diabetic Retinopathy (DR) Detection Techniques. *Approaches and Applications of Deep Learning in Virtual Medical Care*, pp.52-80.
19. Datta, N.S., Dutta, H.S., Majumder, K., Chatterjee, S. and Wasim, N.A., 2022. An improved method for automated identification of hard exudates in diabetic retinopathy disease. *IETE Journal of Research*, *68*(1), pp.611-621.
20. Senapati, R.K., 2022. Bright lesion detection in color fundus images based on texture features. *Bulletin of Electrical Engineering and Informatics*, *5*(1), pp.92-100.
21. Wan, S., Liang, Y. and Zhang, Y., 2021. Deep convolutional neural networks for diabetic retinopathy detection by image classification. *Computers & Electrical Engineering*, *72*, pp.274-282.
22. Chowdhury, A.R., Chatterjee, T. and Banerjee, S., 2019. A random forest classifier-based approach in the detection of abnormalities in the retina. *Medical & biological engineering & computing*, *57*, pp.193-203.